

A Novel Approach to Collision-Induced Dissociation (CID) for Ion Mobility-Mass Spectrometry Experiments

Christopher Becker, Francisco A. Fernandez-Lima, Kent J. Gillig, William K. Russell, Stephanie M. Cologna, and David H. Russell

The Laboratory for Biological Mass Spectrometry, Department of Chemistry, Texas A and M University, College Station, Texas, USA

Collision induced dissociation (CID) combined with matrix assisted laser desorption ionization-mobility-mass spectrometry (MALDI-IM-MS) is described. In this approach, peptide ions are separated on the basis of mobility in a 15 cm drift cell. Following mobility separation, the ions exit the drift cell and enter a 5 cm vacuum interface with a high field region (up to 1000 V/cm) to undergo collisional activation. Ion transmission and ion kinetic energies in the interface are theoretically evaluated accounting for the pressure gradient, interface dimensions, and electric fields. Using this CID technique, we have successfully fragmented and sequenced a number of model peptide ions as well as peptide ions obtained by a tryptic digest. This instrument configuration allows for the simultaneous determination of peptide mass, peptide-ion sequence, and collision-cross section of MALDI-generated ions, providing information critical to the identification of unknown components in complex proteomic samples. (*J Am Soc Mass Spectrom* 2009, 20, 907–914) © 2009 American Society for Mass Spectrometry

Incorporation of post-ionization, gas-phase separations with matrix assisted laser desorption/ionization time-of-flight mass spectrometry (MALDI-TOFMS) represents a significant advance in bioanalytical research, especially studies of proteomics [1, 2] and imaging mass spectrometry [3, 4]. Ion mobility-mass spectrometry (IM-MS) offers several advantages over traditional MS, including increased dynamic range [5], discrimination against chemical noise [5, 6], the ability to separate geometric isomers [7], and separation of ions based on composition and charge state [1, 8]. The cumulative result is highly sensitive, information-rich datasets that are unique to IM-MS techniques. For example, a single IM-MS separation can provide peptide molecular weights (peptide mass-fingerprint), ion-neutral collision cross-sections, and residue specific identification of post-translational modifications (PTMs) [1, 2].

When coupled to fragment ion analysis for determination of primary structure, IM-MS adds a “per sample” throughput advantage over traditional MALDI-MS/MS techniques. That is, the ion mobility spectrometry (IMS) separation provides a temporal correlation between the precursor and product ions, circumventing the need to pre-select each precursor

mass of interest [1, 9, 10]. A number of fragmentation techniques have been previously developed with IM-MS; including photodissociation [11], surface-induced dissociation (SID) [12, 13], and collision-induced dissociation (CID) [10, 14]. Among the available fragmentation techniques, CID is the most widely used owing to the robust nature of the experiment and the high level of sequence coverage obtained. CID is also readily adapted to IMS experiments owing to the presence of a buffer gas at elevated pressures in the IMS cell. Clemmer and coworkers have demonstrated two approaches to CID fragmentation of ions as they exit the mobility cell: (1) by applying a high electric field between the drift tube and mass analyzer [10], and (2) a split-field drift cell design [14]. Additionally, Waters Corporation has introduced an rf ion guide as an interface for their traveling-wave mobility cell that is CID capable [15, 16]. Smith and coworkers have also demonstrated CID of mobility-separated ions using a ramped voltage gradient between two short quadrupoles [9]. Here, we describe a different approach to IM-CID-MS that is compatible with MALDI and periodic-field drift cells. The low-energy, multi-collision CID occurs in the IM-MS vacuum interface, and takes advantage of the existing pressure gradient (from Torr to milli Torr) by varying the field strength over a small region of the interface, thus collisionally activating ions exiting the IMS cell.

Address reprint requests to Dr. D. H. Russell, Laboratory for Biological Mass Spectrometry, 3255 TAMU, College Station, TX 77843-3255, USA. E-mail: russell@mail.chem.tamu.edu

Experimental

The peptides and proteins used in these studies were purchased from Aldrich (St. Louis, MO) and used as received. Samples were prepared for MALDI analysis using a dried droplet method by diluting the peptides (0.5 mg/mL in distilled and deionized H₂O) 1:10 with α -cyano-4-hydroxycinnamic acid (7 mg/mL in methanol with 0.1% TFA) resulting in \sim 500:1 M matrix-to-analyte ratio. Trypsin digestion of lysozyme was performed using standard protocols as described elsewhere [17]. Briefly, lysozyme was thermally-denatured at 90 °C for 20 min, then enzymatically-digested with sequencing-grade trypsin (Promega, Madison, WI) in a 1: 40 (wt/wt) enzyme to analyte ratio at 37 °C for 4 h. The digest solution was then quenched at -10 °C for 10 min and 1 μ L aliquots were prepared for IM-CID-MS analysis as described above.

The IM-MS spectrometer used in these studies has been described previously [6, 18–20]. Briefly, MALDI was performed using a frequency-tripled solid-state Nd:YAG laser (355 nm, Power Chip) operated at a frequency of 300 Hz. IMS separations occur in a 15 cm-long periodic-field drift cell, built in collaboration with Ionwerks (Houston, TX) [20] maintained at \sim 3 Torr with helium as a buffer gas (UHP grade). The drift cell is composed of periodically alternating higher-field/lower-field regions defined by the voltage drop across the drift cell and the electrode spacing [20]. Typical IMS field strength/pressure (E/p) ratios were 10–15 V cm⁻¹ torr⁻¹ and all measurements were performed at room temperature (ca. 298 K). Ions exit the drift cell through a 500 μ m diameter aperture and enter the interface, which consists of a 5-cm long, periodic-field, stacked-ring ion guide. The interface serves to radially confine and transfer ions from the exit aperture of the drift cell to the high-vacuum region of the orthogonal-TOF source. The electrode configuration of the interface is similar to the periodic-field drift cell; however, the pressure in this region is not constant and the exit aperture is defined by the i.d. of the ring electrodes (i.e., it is an open-ended drift tube rather than a drift cell with a small aperture at the end). A SIMION schematic of the interface is contained in Figure 1. The electric field across the interface is controlled by three high-voltage power supplies (UltraVolt, Inc., Ronkonkoma, NY) variable from 0 TO 450 V. The interface is divided into three regions, I, II, and III, as shown in Figure 1. For general IM-MS operation, the electric field across all three regions is constant (30–50 V cm⁻¹). To perform CID, the electric field in region II is increased (600–1000 V cm⁻¹) while maintaining the same electric-field strength in the other two regions as used for non-CID IM-MS experiments.

The TOF mass spectra were externally calibrated using a C60 and C70 mixture (Sigma, St. Louis, MO). The 2D IM-MS data were acquired and processed using custom software (Ionwerks Inc.). Analysis of 1-D fragment ion spectra was performed using Data Explorer

(Applied Biosystems, Inc., Foster City, CA) with 0.20 Da mass accuracies for peak detection and a signal-to-noise peak-detection threshold of 3.

To simulate the ion transmission and ion activation that occurs in the interface region, we first modeled the pressure gradient across the interface using Fluent 6.2.16 (Fluent, Inc., Lebanon, NH) [21]. The resulting pressure gradient was then incorporated into a SIMION model of the interface to simulate ion transmission and ion kinetic energy. For the pressure simulation in Fluent, we assumed an ideal-gas behavior and determined the specific heat capacity (c_p), thermal conductivity, and viscosity parameters using a helium–helium Lennard-Jones interaction potential as defined by kinetic theory. Specifically, an inter-nuclear distance of 2.96 Å and an interaction energy of 10.98 K were used to describe the helium–helium Lennard-Jones interaction potential [22]. Ion transmission and ion kinetic energies in the interface were modeled using a SIMION 3D (Scientific Instrument Services, Inc., Ringoes, NJ) user developed program (version 8.0) [23]. Ion trajectories were calculated using an Elastic Hard Sphere Scattering model (EHSS) for the ion-helium collisions [24]. The ion kinetic energy (KE) and number of collisions were recorded as a function of the distance along the axis of the interface.

Results and Discussion

We previously demonstrated the advantages of using an IM-MS instrument for acquisition of MS/MS data, using either SID or CID, without the need for precursor ion selection since they are already separated in the mobility domain [12, 13, 25]. When using IM-SID-MS, ions exiting the IMS cell are accelerated towards the SID surface positioned in the TOF ion source, and fragmentation thresholds are achieved by increasing the kinetic energy of the ions before impacting the SID surface. We also demonstrated that our IM-MS interface is ideally suited for low-energy, multicollision CID because the increasing E/P ratio permits collisional activation of ions when the voltage drop across the interface is increased [25]. Ion transmission in the interface is also proportional to E/P, i.e., collisional cooling is required to maintain ion focusing. In the current work, we use a single high field region and SIMION ion trajectory calculations to improve the ion transmission of the interface during CID. The end goal of this work is to achieve CID of mobility-separated, MALDI-generated ions in the mass range required for proteolytic digests while maintaining the transmission characteristics of the existing interface.

To optimize the interface for CID, we examined a number of electrostatic configurations using SIMION models. Figure 1 contains plots of ion trajectories obtained from SIMION for the electrostatic configuration that returned the best results for ion activation and transmission. To simulate conditions for low-field IMS ion transmission (no CID), a 180 V drop is applied across the interface (10 V per electrode, Figure 1b) and

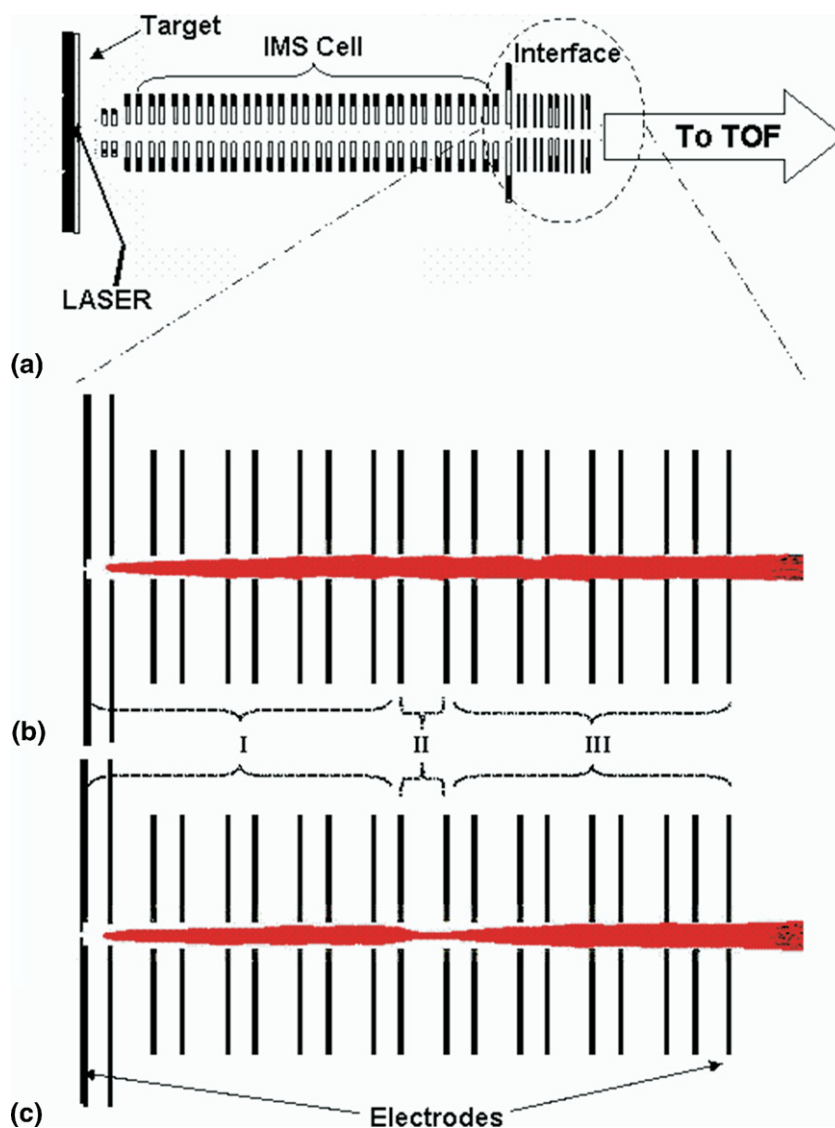


Figure 1. (a) Schematic of the MALDI/IMS drift cell and vacuum interface. A cutaway view of the interface is expanded in (b) and (c). Pre-CID, CID, and post-CID regions of the interface are indicated by brackets and labeled regions "I, II, and III," respectively. (b) SIMION ion trajectories are shown for 500 ions having 1700 m/z . A 10 V drop is applied across each electrode. (c) A 10 V drop per electrode is applied in regions I and III and a 400 V drop is applied across region II to simulate CID conditions. Ion trajectories are shown for 1700 m/z ions changing to 1000 m/z fragment ions at the midpoint of region II. Each collision between an ion and buffer gas molecule is indicated by a red mark; representative collision cross-sections were obtained from the literature [33].

ions exiting the mobility cell are focused into a beam with dimensions that are defined by E/P and the i.d. of the electrodes [20]. CID conditions are simulated by applying a 400 V drop (~ 800 V/cm) across region II (Figure 1c); as shown below, these field strengths are sufficiently high to induce collisional activation, which results in abundant fragment ion spectra. Note that the small i.d. of the interface electrodes (1.3 mm) shield the remaining portion of the interface from region II, creating a localized high-field region for collisional activation of ions. Thus, it is possible to perform CID in our interface without the use of field-confining grids, which may decrease ion transmission at the elevated pressures typical of IMS experiments (1–10 Torr).

To accurately model ion transmission under the CID conditions outlined above, the mass and collision cross-section of each ion was changed at the midpoint of region II to simulate the formation of a lower-mass fragment ion. To determine the efficiency of fragment ion transmission over the mass range of interest, we simulated ion transmission efficiencies for m/z 100–1700 fragment ions. The results of these simulations reveal 80% to 90% transmission for fragment ions between 500 and 1700 m/z , and 40% to 80% transmission for fragment ions between 100 and 500 m/z , providing evidence that this technique is capable of transmitting ions over the m/z region of interest for peptide fragmentation. Figure 1c illustrates the ion trajectories for a m/z 1700

ion fragmenting to a m/z 1000 fragment ion in the CID region. These data demonstrate that precursor and fragment ions are efficiently transmitted under these conditions.

Figure 2 contains a plot of KE versus the axial ion position in the interface. Note that the value of KE reflects low-field conditions (below 2 eV) in region I of the interface (Figure 2); however, upon entering region II, KE increases to over 140 eV, which is shown to be sufficient to induce peptide fragmentation as described below (Figure 3). Ions exiting region II experience cooling collisions with the He buffer gas and the KE returns to lower, nonactivation values in region III. A small increase in KE (to ~ 6 –7 eV) is noted near the end of the interface owing to the rapid pressure drop in this region (Figure 3, inset). The pressure drop results in a gradually increasing E/p as ions exit the vacuum interface, which facilitates efficient ion transmission to the TOF source. The data shown in Figure 2 suggests that by varying the electric fields in various regions of the ion mobility drift cell or interface, we can control the kinetic energy such that ions can be separated on the basis of collision cross-section or collisionally activated to energies above the dissociation threshold to perform energy-dependent fragmentation studies (e.g., collisional activation-IMS, IMS-collisional activation-IMS, etc.).

We used fibrinopeptide A (m/z 1536 for the $[M + H]^+$ ion) to demonstrate CID in the IM-MS interface. The CID experiment was performed by applying 400 V across region II and the corresponding IM-CID-MS spectrum was recorded. The lower panel of Figure 3 contains a plot of ion arrival time distribution (ATD) versus m/z obtained with the CID experiment, and

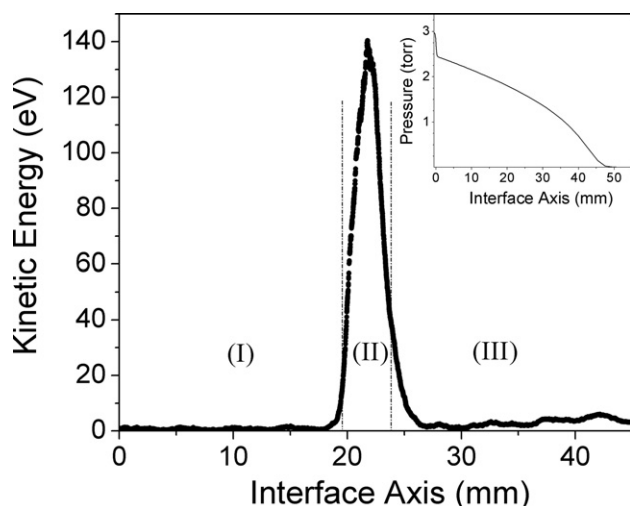


Figure 2. The ion kinetic energy (eV) is shown for 1700 m/z ions with a collision cross-section of 350 \AA^2 as they traverse the length of the IM-MS interface. The circles represent the kinetic energy of the ion after each ion-neutral collision. The values of the electrostatic field were 34, 800, and 34 V/cm in regions I, II, and III, respectively. The simulated pressure gradient across the interface is inset (simulated using 3 torr of Helium as the operating pressure inside the drift cell).

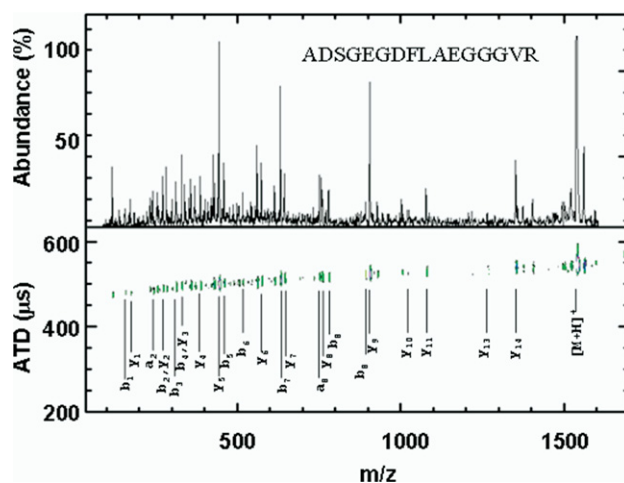


Figure 3. (bottom) Plot of m/z versus ATD containing IM-CID-MS data for fragmentation of fibrinopeptide A, and (top) Mass spectra obtained by integrating across the narrow ATD window corresponding to precursor and fragment ions of fibrinopeptide A.

abundant fragment ions are detected. In the upper panel of Figure 3, a 1D mass spectrum is obtained by integrating across the ATD interval of 470–550 μs . The fragment ion spectrum is essentially the same as that obtained by using MALDI TOF-TOF, i.e., the spectrum contains a near complete series of y -type fragment ions and a partial series of a - and b -type fragment ions. In addition, fragment ions are also present, which correspond to internal fragment ions and ions formed by loss of small neutrals from a -, b -, and y -type fragment ions (i.e., loss of H_2O and NH_3).

It is noted that fragment ions are detected showing a small deviation towards shorter ATDs (relative to the

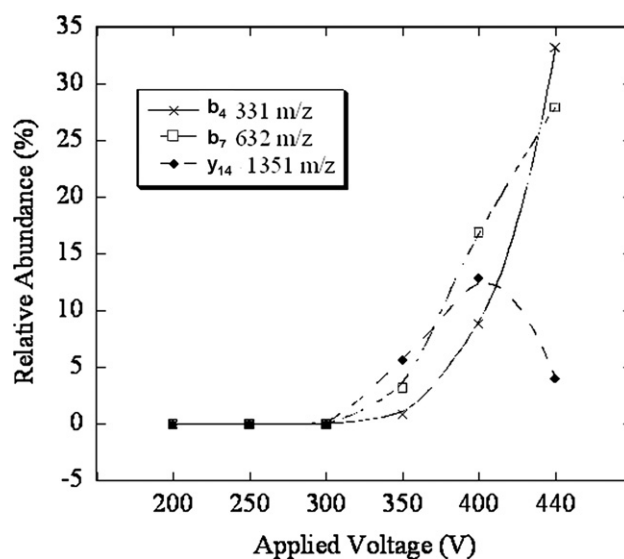


Figure 4. Plot of relative abundance versus applied voltage for selected fragment ions from fibrinopeptide A: b_4 (ADSG), b_7 (ADSGEGD), and y_{14} (SGEGDFLAEGGGVR). Smoothed curve fits are added to guide the eye.

$[M + H]^+$ ions) in Figure 3, which arises as a consequence of the m/z -dependent flight times to the TOF source after the fragment ions are formed. This ATD offset is inherent in IM-CID-MS experiments and can be corrected by applying a nonlinear calibration, i.e., the ion transit time to the TOF ion source is proportional to the square root of the ion's mass. However, this deviation is typically small (less than 13% between m/z 100–1600) and can be ignored, considering the relative deviation from a precursor ATD is a continuous function of m/z .

An advantage of performing CID experiments using this technique is that the kinetic energy of the ion can be accurately controlled, thus we should be able to perform energy-resolved CID experiments. For example, at

low KE values, we detect primarily higher m/z fragment ions, and as KE is increased, the abundances of lower m/z fragment ions increases, and we see a corresponding decrease in higher m/z fragment ions. The significance of this result is that we can perform experiments to examine dependence of specific fragment ion abundances on the kinetic energy available to the ion in a controlled fashion. As an example, the relative abundances of three selected fragment ions from fibrinopeptide A are plotted as a function of applied voltage in Figure 4. These data show a high degree of control over fragmentation, which may prove useful for optimizing CID spectra and sequence information.

Figure 5 contains CID spectra of bradykinin, angiotensin I, and α melanocyte stimulating hormone. Each

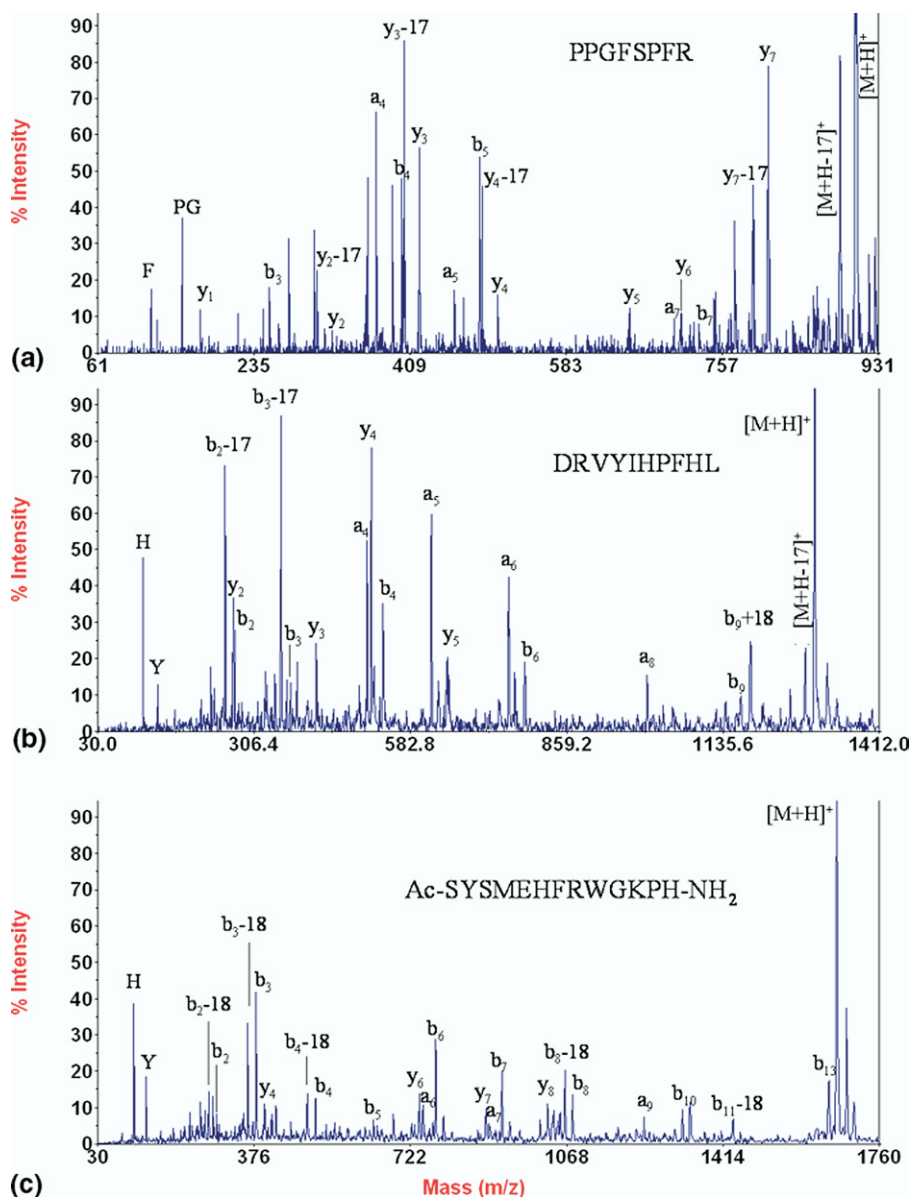


Figure 5. CID spectra for three peptides obtained by integrating across the narrow ATD window corresponding to respective precursor and fragment ions: (a) bradykinin 2-9 collected at 300 V, (b) angiotensin I collected at 360 V, and (c) α melanocyte stimulating hormone collected at 440 V.

spectrum was acquired at a *KE*, which produces a high abundance of fragment ions to obtain the best sequence coverage. The dominant fragment ions in each spectrum were *a*-, *b*-, and *y*-type fragment ions and fragment ions with neutral losses of H₂O and NH₃ also observed. The IM-CID-MS spectra in Figure 5 were compared with spectra obtained on commercial MALDI-TOF-CID-TOF instruments (data not shown), and the fragment ion spectra from these two techniques show essentially the same sequence coverage; the main difference being that the IM-CID-MS method produces a greater abundance of internal fragment ions as expected for multi-collision CID.

The analysis of a more complex proteomic sample using IM-CID-MS is illustrated by data contained in Figure 6, which displays the IM-CID-MS results for a tryptic digest of lysozyme. The sequence coverage for lysozyme from this digest was ~25% and is the same as

that observed by MALDI-TOF analysis, although enhanced sequence coverage by IM-MS has been noted previously [5, 6]. IM-CID-MS fragment-ion spectra for the three prominent lysozyme digest fragments are also depicted in Figure 6. These data (Figure 6) were collected using three different voltage settings. Under the selected CID conditions, fragment ion abundances were maximized for the three precursor ions and a good correlation between fragment and parent ions is obtained (Figure 6, i-iii). An advantage of this IM-MS approach is that the fragment ions from multiple precursor ions are resolved in the mobility dimension, which allows simultaneous collection of fragmentation spectra over a large *m/z* range without necessitating multiple experimental runs requiring mass selection for each precursor ion of interest. This IM-CID-MS platform has the potential to obtain energy-dependent CID spectra of conformational isomers (such as those ob-

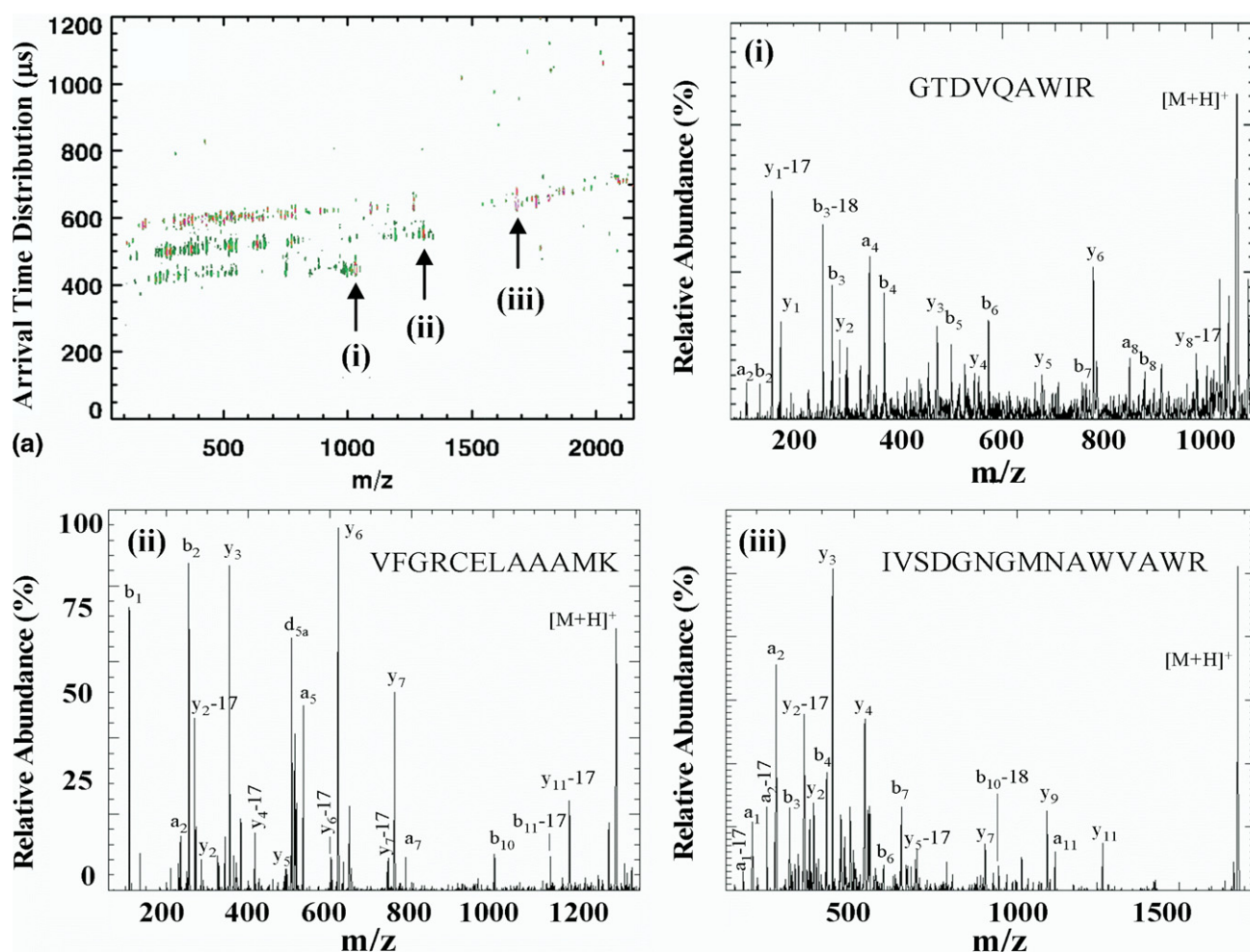


Figure 6. (a) Plot of *m/z* versus ATD containing IM-CID-MS data for fragmentation of peptides from a lysozyme digest containing ion signal from three prominent tryptic peptides: (i) GTDVGAWIR, (ii) VFGRCELAAAMK, and (iii) IVSDGNGMNAWVAWR. (i) Mass spectra obtained by integrating across the narrow ATD window corresponding to precursor and fragment ions of GTDVGAWIR (optimized at 280 V), (ii) Mass spectra obtained by integrating across the narrow ATD window corresponding to precursor and fragment ions of VFGRCELAAAMK (optimized at 360 V), and (iii) Mass spectra obtained by integrating across the narrow ATD window corresponding to precursor and fragment ions of IVSDGNGMNAWVAWR (optimized at 440 V).

served for bradykin 1-5) [26] as well as provide rapid screening for PTMs [27, 28] to acquire data dependent MS/MS spectra. In previous work we have demonstrated that tryptic peptides that differ in mass by ~10 Da (<1%) are easily separated by IMS owing to conformational differences, and can be simultaneously sequenced by IM-MS fragmentation techniques [1]. A number of approaches for enhancing IMS separations are also available, including selection of buffer gases [29], variation in the IMS field strength [30], and the addition of various bath-gas and mobility-shift reagents [31], [32].

Conclusion

A new CID-capable IM-MS interface has been theoretically and experimentally described. Simulations incorporating the ion kinetic energy show that voltages sufficient to induce fragmentation can be applied to the interface, while conserving high transmission for precursor and fragment ions. CID of peptide ions was demonstrated for several model peptides and peptides from a proteolytic digest. It is also possible to obtain spectra over a range of applied voltages to enhance ion signal of all fragments, similar to the technique described recently by Smith and coworkers [9]; although a single optimized voltage is generally sufficient to produce fragment ions over the entire m/z range of interest. For example, a 400 V drop across region II of the interface was sufficient to generate all of the fragment ions for fibrinopeptide A between 1400 and 100 m/z that are observed over a range of voltage settings. The results presented in this work demonstrate that efficient dissociation can be observed and illustrates the potential to perform energy-dependent fragmentation studies using a periodic-field drift cell design. This approach provides a relatively simple way to generate mobility-separated fragmentation spectra to sequence peptides from biological samples while maintaining the high-resolution and sensitivity of the IMS separation.

Acknowledgments

The authors acknowledge support for this research by the U.S. Department of Energy, Division of Chemical Sciences/BES (DE-FG-04ER-15,520), the National Science Foundation-Major Research Instrumentation Grant (CHE-0521216), and the Robert A. Welch Foundation (A-1176). The authors also acknowledge many helpful discussions with Tom Egan and Al Schultz at IonWerks, Inc., Houston, Texas.

References

- McLean, J. A.; Ruotolo, B. T.; Gillig, K. J.; Russell, D. H. Ion Mobility-Mass Spectrometry: A New Paradigm for Proteomics. *Int. J. Mass Spectrom.* **2005**, *240*, 301–315.
- Liu, X.; Valentine, S. J.; Plasencia, M. D.; Trimpin, S.; Naylor, S.; Clemmer, D. E. Mapping the Human Plasma Proteome by SCX-LC-IMS-MS. *J. Am. Soc. Mass Spectrom.* **2007**, *18*, 1249–1264.
- Jackson, S. N.; Ugarov, M.; Egan, T.; Post, J. D.; Langlais, D.; Schultz, J. A.; Woods, A. S. MALDI-Ion Mobility-TOFMS Imaging of Lipids in Rat Brain Tissue. *J. Mass Spectrom.* **2007**, *42*, 1093–1098.
- McLean, J. A.; Ridenour, W. B.; Caprioli, R. M. Profiling and Imaging of Tissues by Imaging Ion Mobility-Mass Spectrometry. *J. Mass Spectrom.* **2007**, *42*, 1099–1105.
- Ruotolo, B.; Gillig, K. J.; Stone, E.; Russell, D. H.; Fuhrer, K.; Gonin, M.; Schultz, A. Analysis of Protein Mixtures by Matrix-Assisted Laser Desorption Ionization-Ion Mobility-Orthogonal-Time-of-Flight Mass Spectrometry. *Int. J. Mass Spectrom.* **2002**, *219*, 253–267.
- Gillig, K. J.; Ruotolo, B.; Stone, E. G.; Russell, D. H.; Fuhrer, K.; Gonin, M.; Schultz, A. J. Coupling High-Pressure MALDI with Ion Mobility/Orthogonal Time-of-Flight Mass Spectrometry. *Anal. Chem.* **2000**, *72*, 3965–3971.
- Wu, C.; Siems, W. F.; Hill, H. H. Separation of Isomeric Peptides Using Electrospray Ionization/High Resolution Ion Mobility Spectrometry. *Anal. Chem.* **2000**, *72*, 391–395.
- Valentine, S. J.; Kulchania, M.; Barnes, C. A. S.; Clemmer, D. E. Multidimensional Separations of Complex Peptide Mixtures: A Combined High-Performance Liquid Chromatography/Ion Mobility/Time-of-Flight Mass Spectrometry Approach. *Int. J. Mass Spectrom.* **2001**, *212*, 97–109.
- Baker, E. S.; Tang, K.; Danielson, W. F. III.; Prior, D. C.; Smith, R. D. Simultaneous Fragmentation of Multiple Ions Using IMS Drift Time Dependent Collision Energies. *J. Am. Soc. Mass Spectrom.* **2008**, *19*, 411–419.
- Lee, Y. J.; Hoaglund-Hyzer, C. S.; Taraszka, J. A.; Zientara, G. A.; Counterman, A. E.; Clemmer, D. E. Collision-Induced Dissociation of Mobility-Separated Ions Using an Orifice-Skimmer Cone at the Back of a Drift Tube. *Anal. Chem.* **2001**, *73*, 3549–3555.
- McLean, J. A.; Gillig, K. J.; Ruotolo, B. T.; Ugarov, M. V.; Bensaoula, H.; Egan, T. F.; Schultz, J. A.; Russell, D. H. Ion Mobility-Photodissociation (213 nm)-Time-of-Flight Mass Spectrometry for Simultaneous Peptide Mass Mapping and Peptide Sequencing. *Proceedings of the 51st ASMS Conference*, 2003.
- Stone, E.; Gillig, K. J.; Ruotolo, B.; Fuhrer, K.; Gonin, M.; Schultz, A.; Russell, D. H. Surface-Induced Dissociation on a MALDI-Ion Mobility-Orthogonal Time-of-Flight Mass Spectrometer: Sequencing Peptides from an "In-Solution" Protein Digest. *Anal. Chem.* **2001**, *73*, 2233–2238.
- Stone, E. G.; Gillig, K. J.; Ruotolo, B. T.; Russell, D. H. Optimization of a Matrix-Assisted Laser Desorption Ionization-Ion Mobility-Surface-Induced Dissociation-Orthogonal-Time-of-Flight Mass Spectrometer: Simultaneous Acquisition of Multiple Correlated MS1 and MS2 Spectra. *Int. J. Mass Spectrom.* **2001**, *212*, 519–533.
- Valentine, S. J.; Koeniger, S. L.; Clemmer, D. E. A Split-Field Drift Tube for Separation and Efficient Fragmentation of Biomolecular Ions. *Anal. Chem.* **2003**, *75*, 6202–6208.
- Giles, K.; Pringle, S. D.; Worthington, K. R.; Little, D.; Wildgoose, J. L.; Bateman, R. H. Applications of a traveling wave-based radio-frequency-only stacked ring ion guide. *Rapid Commun. Mass Spectrom.* **2004**, *18*, 2401–2414.
- Pringle, S. D.; Giles, K.; Wildgoose, J. L.; Slade, S. E.; Thalassinou, K.; Bateman, R. H.; Bowers, M. T.; Scrivens, J. H. An Investigation of the Mobility Separation of Some Peptide and Protein Ions Using a New Hybrid Quadrupole/Traveling Wave IMS/o-TOF Instrument. *Int. J. Mass Spectrom.* **2007**, *261*, 1–12.
- Park, Z.-Y.; Russell, D. H. Thermal Denaturation: Peptide Mass Mapping. *Anal. Chem.* **2000**, *72*, 2667–2670.
- Gillig, K.J.; Russell, D.H. Periodic field focusing ion mobility spectrometer. U.S. Patent 6639213, 2003.
- Gillig, K. J.; Ruotolo, B. T.; Stone, E. G.; Russell, D. H. An Electrostatic Focusing Ion Guide for Ion Mobility-Mass Spectrometry. *Int. J. Mass Spectrom.* **2004**, *239*, 43–49.
- Schultz, J. A.; Raznikov, V.; Egan, T. F.; Ugarov, M. V.; Tempez, A. Ion Mobility TOF/MALDI/MS Using Drift Cell Alternating High and Low Electrical Field Regions. U.S. Patent 7223969, 2007.
- CFD Fluent, Fluent Inc., <http://www.fluent.com/software/index.htm>.
- Anderson, J. B. An Exact Quantum Monte Carlo Calculation of the Helium-Helium Intermolecular Potential. *J. Chem. Phys.* **2001**, *115*, 4546–4548.
- SIMION 3D, Scientific Instrument Services, Inc., <http://www.simion.com>.
- Ding, J.; Sudakov, M.; Kumashiro, S. A Simulation Study of the Digital Ion Trap Mass Spectrometer. *Int. J. Mass Spectrom.* **2002**, *221*, 117–138.
- Fernandez-Lima, F.A.; Becker, C.; Gillig, K.J.; Russell, W.K.; Tichy, S.E.; Russell D.H. Ion Mobility-Mass Spectrometer Interface for Collisional Activation of Mobility Separated Ions. *Anal. Chem.*, Article ASAP, DOI: 10.1021/ac801919n.
- Sawyer, H. A.; Marini, J. T.; Stone, E. G.; Ruotolo, B. T.; Gillig, K. J.; Russell, D. H. The Structure of Gas-Phase Bradykinin Fragment 1-5 (RPPGF) Ions: An Ion Mobility Spectrometry and H/D Exchange Ion-Molecule Reaction Chemistry Study. *J. Am. Soc. Mass Spectrom.* **2005**, *16*, 893–905.
- Ruotolo, B. T.; Gillig, K. J.; Woods, A. S.; Egan, T. F.; Ugarov, M. V.; Schultz, J. A.; Russell, D. H. Analysis of Phosphorylated Peptides by Ion Mobility-Mass Spectrometry. *Anal. Chem.* **2004**, *76*, 6727–6733.
- Ruotolo, B. T.; Verbeck, G. F.; Thomson, L. M.; Woods, A. S.; Gillig, K. J.; Russell, D. H. Distinguishing Between Phosphorylated and Nonphosphorylated Peptides with Ion Mobility-Mass Spectrometry. *J. Proteome Res.* **2002**, *1*, 303–306.
- Ruotolo, B. T.; McLean, J. A.; Gillig, K. J.; Russell, D. H. Peak Capacity of Ion Mobility Mass Spectrometry: The Utility of Varying Drift Gas Polarizability for the Separation of Tryptic Peptides. *J. Mass Spectrom.* **2004**, *39*, 361–367.

30. Ruotolo, B. T.; McLean, J. A.; Gillig, K. J.; Russell, D. H. The Influence and Utility of Varying Field Strength for the Separation of Tryptic Peptides by Ion Mobility-Mass Spectrometry. *J. Am. Soc. Mass Spectrom.* **2005**, *16*, 158–165.
31. Hilderbrand, A. E.; Myung, S.; Clemmer, D. E. Exploring Crown Ethers as Shift Reagents for Ion Mobility Spectrometry. *Anal. Chem.* **2006**, *78*, 6792–6800.
32. Dwivedi, P.; Ching, W.; Matz, L. M.; Clowers, B. H.; Siems, W. F.; Hill, H. H. Gas-Phase Chiral Separations by Ion Mobility Spectrometry. *Anal. Chem.* **2006**, *78*, 8200–8206.
33. Tao, L.; Mclean, J. R.; Mclean, J. A.; Russell, D. H. A Collision Cross-Section Database of Singly-Charged Peptide Ions. *J. Am. Soc. Mass Spectrom.* **2007**, *18*, 1232–1238.